PMC Physics B

PhysMath Central

Research article

Open Access

Near-threshold electron-impact excitation of argon studied with the time-of-flight technique

Subhendu Mondal[1], Julian Lower*[1], Stephen J Buckman[1], Robert P McEachran[1], Gustavo Garcia[2], Oleg Zatsarinny[3] and Klaus Bartschat[3]

Address: [1]Centre for Antimatter-Matter Studies, Research School of Physical Sciences and Engineering, Australian National University, Canberra, ACT 0200, Australia, [2]Instituto de Fisica Fundamental, CSIC, Serrano 113-bis, 28006, Madrid, Spain and [3]Department of Physics and Astronomy, Drake University, Des Moines, IA, USA

Email: Subhendu Mondal - justsm@gmail.com; Julian Lower* - Julian.Lower@anu.edu.au; Stephen J Buckman - stephen.buckman@anu.edu.au; Robert P McEachran - rpm107@anu.edu.au; Gustavo Garcia - g.garcia@imaff.cfmac.csic.es; Oleg Zatsarinny - oleg_zoi@yahoo.com; Klaus Bartschat - klaus.bartschat@drake.edu

* Corresponding author

Published: 18 December 2009

PMC Physics B 2009, **2**:3 doi:10.1186/1754-0429-2-3

Received: 5 November 2009
Accepted: 18 December 2009

This article is available from: http://www.physmathcentral.com/1754-0429/2/3

Abstract

Absolute angle-differential cross-section data are presented for excitation of the $3p^5 4s$ manifold in argon by electron impact. The investigation focuses on the near-threshold region, where previous studies have revealed persistent disparities between measurements and theoretical predictions. For the present experiment, the time-of-flight (TOF) technique is employed. This method allows for scattered electrons to be measured over a broad range of energies with a constant transmission, thereby eliminating a potential major source of error in relating relative intensities of elastic and inelastic transitions inherent to other experimental techniques. The present experimental data are compared to theoretical results obtained in relativistic distorted-wave and various *R*-matrix (close-coupling) approaches, as well as to other recently published experimental data.

PACS Codes: 34.80.Dp

1. Background

The accurate determination and understanding of electron-impact-induced atomic collision processes is important for a number of reasons. From a practical perspective, the modelling of many systems of environmental and technological interest relies on the incorporation of cross-section data to describe collision processes at the microscopic scale. These cross sections predict reaction rates for the range of possible collision outcomes comprising elastic scattering, excita-

tion, and ionization. Thus the provision of precise cross-section data is vital to these applications. Sometimes, particularly in elastic scattering and excitation from the ground state, cross sections can be measured more accurately than they can presumably be calculated. On the other hand, measurements involving optically unstable initial states can be very difficult and are often impossible with currently available experimental techniques.

Experimental benchmark data, therefore, may provide a crucial touchstone to both assess and to drive new developments in atomic collision theory and enhance its predictive powers. From a broader perspective, studies of electron-atom collisions contribute to our understanding of the electronic structure of matter by providing a well-defined testing ground to explore the many-body behaviour of many-electron systems.

In the area of electron-atom collisions, the electron-noble-gas system has been a prime focus of study over many years. From the experimental perspective, these non-reactive gases can be easily handled and do not contaminate sensitive apparatuses. As a consequence, they are particularly conducive to the measurement of accurate cross-section data, which can assist in the development of theory for all atomic species, including those whose reactivity renders experiment infeasible. The present study concerns the excitation of argon atoms close to threshold, for which discrepancies between experiment and theory have persisted over a number of decades. Argon represents the most ubiquitous noble gas of the earth's atmosphere, comprising around 0.93% of its composition. It is used in a variety of applications including argon lasers, plasma processing, incandescent lighting, and welding. Here we focus on the electron-impact-induced excitation of the $3p^5 4s$ manifold from the $3p^6$ ground state. These transitions correspond to excitation of the lowest excited states comprising four energetically separated levels.

The near-threshold region for electron-atom scattering is problematic for both theory and experiment for a variety of reasons. For theory, perturbative approaches break down in the neighbourhood of an excitation threshold where the energy E_s of the scattered electron is very low. Defining E_j as the excitation energy of the atomic state j with respect to the atomic ground-state energy and E_p as the energy of the projectile electron, E_s is related to these quantities through $E_s = E_p - E_j$. The calculations are further complicated by the wealth of resonances frequently appearing in the near-threshold region. For argon these occur predominantly between ~11.5 eV and the threshold for single ionization at 15.8 eV. Describing the cross section in regions where both resonant and non-resonant processes compete is a more challenging theoretical problem than describing regions where the direct excitation channel dominates.

Measurements are complicated for other reasons. Firstly, the magnitude of the excitation cross section for transitions to each state j decreases as the projectile energy E_p approaches the excitation threshold at $E_p = E_j$, thus leading to lower count rates and increased statistical error. Secondly, the number of background electrons, resulting from the generation of low-energy secondary elec-

trons produced, for example, by collision of the primary beam with the beam dump (Faraday cup), is strongly weighted towards low energies. These electrons are difficult to suppress and can form a large background upon which the signal from the target gas is superimposed, thereby increasing statistical errors and rendering the experiment sensitive to any systematic errors in background subtraction. Thirdly, the electron transmission $\eta(E_s)$ of many analyzers becomes strongly energy dependent as $E_s \to 0$. The electron transmission is defined as the probability that a scattered electron, upon entering an analyzer, will reach the detector. For transitions to a state j, this situation occurs as the incident beam energy $E_p \to E_j$. Characterization of $\eta(E_s)$ in the neighbourhood of $E_s = 0$ is a difficult proposition. Crucially, any inaccuracies in the determination of its energy dependence translate directly into uncertainties in deduced differential cross-section (DCS) values. Finally, in the neighbourhood of resonance structures, measured DCSs may be particularly sensitive to the intrinsic energy spread of the primary electron beam and to the accuracy with which its energy is calibrated. This is because the DCSs can change very rapidly with projectile energy E_p in these regions. In such cases, small errors in energy calibration, or the different energy resolutions characterizing different experiments performed at the same nominal impact energy, can potentially lead to significant discrepancies.

Previous measurements for the excitation of the $3p^5 4s$ configuration of argon were summarized by Filipovic *et al* [1,2] and hence will not be repeated here. All the DCS measurements reported in that work were performed at an incident energy E_p of 16 eV or above. At higher values of the impact energy, good agreement was observed between experiment and theoretical predictions. This is not surprising as the accuracy of perturbative approaches and the reliability of experimental data increase with increasing impact energy.

Recently, Khakoo *et al* [3] extended the range of measurements on the electron-argon system much closer to the lowest excitation threshold by presenting measurements reaching down to an impact energy of 14 eV. Furthermore, they resolved the DCSs for the individual transitions to the four levels comprising the $3p^5 4s$ configuration of argon. While good agreement was found between theory and experiment at impact energies above 50 eV, Khakoo *et al* found significant disparities emerging as the threshold was approached.

In an attempt to resolve discrepancies in the near-threshold region, we also performed measurements at the impact energies of 17.5 eV, 15.0 eV, and 14.0 eV considered by Khakoo *et al* [3] and then probed even closer to threshold than previous work by performing a measurement at 12.5 eV, i.e., only about 1 eV from the excitation threshold for the $3p^5 4s\ [3/2]_2^0$ state. In contrast to the measurements of Khakoo *et al* [3], we employ a time-of-flight spectrometer, which is particularly well suited to measuring energy-loss spectra in the near-threshold region due to its uni-

form transmission. We do not, however, resolve the four levels comprising the $3p^5 4s$ manifold of argon as they did and, therefore, compare our results to their summed DCSs.

2. Results and discussion

2.1 Experimental methods

2.1.1 Apparatus

Since the time-of-flight electron spectrometer used for the present series of measurements has been described previously [4], only a brief description will be given here. It comprises a pulsed source of energy-selected electrons, an interaction volume where the pulsed electron projectile beam and the argon target beam intersect, and a field-free drift tube. Scattered electrons drift through the latter tube towards a position- and time-sensitive detector, upon which their temporal and spatial arrival coordinates are recorded.

The primary electron beam is formed from thermionic emission from a grounded thoriated tungsten filament. Electrons, with an initial energy spread of ~0.5 eV, are extracted from the filament by a weak electrostatic field before being focussed into a 180° electrostatic deflector where they are dispersed in space according to their energy. A thin exit slit at the deflector exit selects electrons over a narrow energy band (~0.05 - 0.07 eV for the present measurements) after which they are focussed at 10 eV between two deflector plates terminated by a small 1.5 mm square aperture. Through the application of a time-dependent voltage, the deflector plates produce a train of electron pulses, with a duration selectable between 1 and 10 ns.

We previously explored a number of different pulsing schemes (see [4] and references therein) to optimize the intensity, energy resolution, and temporal properties of the pulses. For the present measurements we use a simple scheme where a bias voltage is applied across the two deflector plates to form a constant electric field between them and to deflect the continuous electron beam, generated by the filament, away from the pulsing-unit exit aperture. A fast periodic ac voltage is then superimposed upon the dc bias voltage to nullify the electric field for short intervals and to allow for the transmission of a train of electron pulses. For the present measurements identical (except for the sign) square-form voltage pulses are applied to each plate simultaneously using a custom-built AVTECH pulse generator. These pulses exhibit a rise time of less than 1 ns, a duration of around 24 ns, and an amplitude of 0.5 V. Taking into account the approximately 16 ns required for the electrons to traverse the length of the deflector plates (30 mm), this results in electron pulses of around 8ns duration. Pulsing is undertaken at a rate of 800 kHz, leading to a duty cycle of ~0.1%. Subsequent electron optics focuses the train of pulses onto the argon target beam at the selected collision energy $E_p = eV_p$. where V_p is the potential at the interaction region. It is set by adjusting the potential of the shielding electrodes that surround it. The argon beam is formed by effusion through a 1 mm internal diameter stainless-steel tube. The overlap between the electron and argon beams defines a localized interaction volume in which collisions

occur. A Faraday cup positioned a short distance behind the interaction region, and mounted on a movable arm, allows for the beam current to be measured.

Scattered electrons of different energy-loss values enter the cone-shaped drift tube and travel towards the detector where their spatial and temporal arrival coordinates are measured. When E_p is below the ionization threshold E_i at 15.8 eV, energy-loss values span from zero (elastic scattering) up to that corresponding to excitation of the highest energetically accessible excited state of the neutral argon atom. When E_p lies above the ionization threshold, as for our measurement at 17.5 eV, energy-loss values extend to the value E_p. Flight times for each detected electron are measured with respect to the arrival time, at the interaction region, of the electron pulse that resulted in its liberation. From a measurement of the electron flight times t for scattered electrons of energy E_s, a measurement of the electron arrival positions (x, y) at the detector, and from the knowledge of the length d of the drift region (209 mm), the angle-differential energy-loss spectra can be derived [4]. The drift tube collects electrons scattered over a 20° cone centred around a mean scattering angle θ_m, which can be adjusted between 55° and 120° by rotating the turntable upon which the electron gun is mounted. With the 20° cone of the drift tube, scattering angles are determined to better than 2°, although data is integrated over a 5° interval for the present measurements to improve the statistics.

Energy calibration of the primary beam is achieved by utilizing a channeltron detector, positioned above the gas jet, to measure the count rate resulting from the detection of metastable argon atoms as the incident-beam energy E_p is scanned. Well-defined resonance-related structures in the metastable-atom excitation function, which have been identified previously and whose energies have been determined to high precision [5], are used to calibrate the energy scale. Furthermore, due to their intrinsically narrow natural energy widths, the resonance structures in the metastable-atom excitation function were also used to determine the energy spread ΔE_p of the primary electron beam, which varied between 50 meV and 70 meV in the present series of measurements.

2.1.2 Measurement procedure and background subtraction

Before extracting DCS data from measured energy-loss spectra, contributions from stray electrons must be extracted. The main component of the stray-electron background results from primary-beam electrons scattering elastically and inelastically from the metal components in the vacuum chamber and from the secondary electrons they generate in the process. To minimize background levels, the Faraday cup was moved out of the path of the primary electron beam once optimal focussing conditions were established and the DCS measurement cycle was about to commence. This allowed the primary electron beam to scatter from the positively-biased mu-metal lining of the vacuum chamber walls located some 500 mm behind the interaction region. This action proved most effective in reducing the number of stray electrons entering the drift tube.

Each experiment consisted of a sequence of alternately performed "signal" and "background" runs. In the signal mode, the gas supply is directed to the capillary located directly below the interaction volume. In the background mode, the gas supply is redirected from this capillary to one of similar dimensions mounted at the chamber periphery. The dimensions of the tubes supplying the two capillaries were carefully matched to ensure identical gas throughput in both modes. Every hour, over the course of an experiment, the measurements alternated between "signal mode" and "background mode", data from each being accumulated for equal times. The subtraction of background from the signal mode data provided an essentially background-free TOF spectrum.

2.1.3 Energy resolution and duty cycle considerations

Many factors determine the total energy resolution ΔE_{tot} with which a TOF spectrometer can resolve energy-loss structure. A detailed description of these and their somewhat complicated relationship can be found in a previous publication [6]. For the present measurements, the major contributing factors are the temporal width Δt of the primary-electron pulse and its intrinsic energy spread ΔE_p. The energy resolution strongly depends on the energy E_s of the measured scattered electrons corresponding to the excitation of the atomic state j of energy E_j above the ground state, where ($E_s = E_p - E_j$).

To explain the present choice of experimental parameters, an approximate mathematical relationship between these three quantities is presented below. In this simplified derivation weak effects due to the finite size of the interaction volume are neglected, as are the finite response time of the timing electronics and the temporal broadening of the electron pulse as it travels towards the interaction volume, resulting from its finite energy width ΔE_p.

The time t for scattered electrons of energy E_s to drift from the interaction region to the detector is given by the expression

$$t = d\sqrt{\frac{m_e}{2E_s}}. \tag{1}$$

Here m_e is the electron mass and d is the drift length (209 mm for an electron impacting the centre of the present extended channelplate detector). The non-linear dispersion of the drift time t with scattered-electron energy E_s, inherent to the TOF technique, is evident from the $E_s^{-1/2}$ dependence. Differentiation of this equation leads to the finite-difference expression:

$$\Delta E_s = -\sqrt{\frac{8}{m_e}}\frac{1}{d}E_s^{3/2}\Delta t. \tag{2}$$

For a monochromatic source of electrons, Eq. (2) shows that for a given pulse length Δt the energy resolution improves with decreasing energy as $E_s^{3/2}$. Thus, not only from the perspective of uniform transmission, but also from the perspective of good energy resolution, the TOF technique is well suited to studies of low-energy electrons as encountered in the present near-threshold study. In reality, the primary beam is not monochromatic, possessing an intrinsic energy spread ΔE_p that will also contribute to the total energy-loss resolution ΔE_{tot}. Hence, $\Delta E_{tot} = g\ (\Delta E_p, \Delta E_s)$ where g is some function.

In the limiting case $E_s \to 0$, it follows that $\Delta E_s \to 0$ and $\Delta E_{tot} \to \Delta E_p$, i.e., the total energy resolution converges to the energy spread of the primary electron beam. Thus, for this case (long drift times), ΔE_{tot} is relatively insensitive to the magnitude of the pulse length Δt as energy-loss structures are well separated in time, as seen from the $E_s^{-3/2}$ dependence of Δt obtained by inverting Eq. (2). In contrast, in the limiting case $\Delta t \to \infty$, $\Delta E_{tot} \to \Delta E_s$. Thus, for higher values of the scattered-electron energies (e.g., as encountered for elastic scattering in the present study), the total energy resolution is dominated by the pulse length Δt, with proportionality achieved in the limiting case $\Delta t \to \infty$, as seen from Eq. (2). Given that the data collection rate is proportional to Δt, its value is chosen as a compromise between improving energy resolution (small Δt) and improving the statistical quality of measurement (Δt large).

Due to the low cross sections encountered in the near-threshold region we operated with longer pulse lengths, in the regime where Δt dominates the energy resolution, to increase the count rates. As a consequence, we were not able to resolve the four individual contributions to the $3p^5 4s$ manifold as achieved by Khakoo *et al* [3]. The results presented below represent a sum over these four states. However, the TOF technique employed in the present experiment has the distinct advantage of exhibiting a uniform analyzer transmission, thus giving us great confidence in the accuracy of our derived DCS data.

2.1.4 Determination of absolute DCS data from TOF spectra

In the case where inelastic cross sections are normalized to elastic scattering, the absolute differential cross section $\mathrm{DCS}_{\mathrm{j}}^{\mathrm{inel}}(\theta)$ for scattering leading to excitation of an inelastic channel j is given by the expression

$$\mathrm{DCS}_{\mathrm{j}}^{\mathrm{inel}}(\theta) = \frac{N_j(\theta)}{N_{el}(\theta)} \frac{\eta(E_p)}{\eta(E_s)} \mathrm{DCS}_{el}(\theta). \tag{3}$$

Here, $N_{el}(\theta)$ is the measured count rate for elastic scattering, $N_j(\theta)$ is the corresponding count rate for excitation to the inelastic channel j, while $\eta(E_p)$ and $\eta(E_s)$ are, respectively, values for the electron transmission at the energies of the projectile and of the scattered electron.

Furthermore, $DCS_{el}(\theta)$ is the DCS for elastic scattering, which is accurately known from both theory and experiment for the present case of e-Ar collisions. As was undertaken by Khakoo *et al* [3] to place their inelastic DCS data on an absolute scale, we employed $DCS_{el}(\theta)$ values obtained by performing a selective average over the absolute elastic DCS data of Srivastava *et al* [7], Panajotovic *et al* [8], Furst *et al* [9], Dubois and Rudd [10], and Andrick (see Furst *et al* [9]) and Williams [11]). We assume $\eta(E_s)/\eta\ (E_p) = 1.0$ for the present work and anticipate errors due to deviations from unity to be very small in light of the excellent agreement obtained previously [12] between well-established theory and inelastic DCS data obtained using the same spectrometer for the much simpler "benchmark" case of electron-helium scattering.

2.2 Theory

Results from several numerical models are presented below. One of those is a relativistic distorted-wave (RDW) calculation. The wavefunctions for the $3p^6$ ground state and the four excited $3p^5 4s$ states, namely (with increasing energy above the ground state and following the $j[K]_J$ coupling scheme [13]) the $(3p^5 4s)\ [3/2]^0_2$, $(3p^5 4s)\ [3/2]^0_1$, $(3p^5 4s')\ [1/2]^0_0$, and $(3p^5 4s')\ [1/2]^0_1$ states, were determined in a single multi-configuration Dirac-Fock calculation. The transition-matrix elements for their excitation were calculated using a first-order relativistic distorted-wave method [14], in which the distorted waves were determined in the static and exchange fields of the final states. The present RDW code contains a much more accurate representation of the exchange interaction in the excited state channel than that originally used in [14]. This should be particularly important at low impact energies.

The other three calculations are all based on the *R*-matrix approach, as an efficient way to solve the close-coupling (CC) equations. In two cases, relativistic effects were accounted for through the one-electron terms of the Breit-Pauli hamiltonian, i.e., as a first-order perturbation calculated with non-relativistic one-electron orbitals. One generally expects this approach to be sufficiently accurate for a light neutral target such as argon with nuclear charge $Z = 18$. This means that inaccuracies in the target wavefunctions are most likely not due to such an approximate treatment of relativistic effects, but rather caused by a lack of accounting for valence and core-valence correlation and by the strong term dependence of individual valence orbitals. Furthermore, shortcomings in the theoretical treatment of the collision process are likely due to an insufficient account of channel coupling to higher Rydberg states and particularly the ionization continuum. This is being tested in the third calculation, which is non-relativistic but accounts for the additional coupling.

As will be summarized below, significant progress has been made in recent years regarding both the problems with the target description and the channel coupling. We begin, however,

with a brief summary of the simplest calculation for which results are presented below. This is the 41-state model developed by Zeman and Bartschat [15]. Specifically, it closely couples the lowest 31 physical target states of Ar (the $3p^6$ ground state plus four states with configuration $3p^5 4s$, ten with configuration $3p^5 4p$, twelve with configuration $3p^5 3d$, and four with configuration $3p^5 5s$), as well as ten pseudo-states with configuration $3p^5 5\overline{p}$. The $5\overline{p}$ pseudo-orbital was introduced in order to address, to some extent at least, the strong term dependence of the 5p orbital in the $3p^5$ manifold. Results from this model, which will be referred to as BPRM-41 below, were shown by Khakoo *et al* [3] to compare with their experimental data.

A major improvement of the target description was achieved in the Breit-Pauli *B*-spline *R*-matrix (BSR) calculations presented by Zatsarinny and Bartschat [16]. Employing basis (*B*-)splines as the underlying, effectively complete numerical basis, the critical step was the use of individually optimized, term-dependent, and hence non-orthogonal orbitals for the 31 physical target states used in the close-coupling expansion. While this BSR-31 model neglects coupling to the target continuum completely, one would expect it to be highly accurate in the near-threshold regime investigated in the present work, with problems most likely to arise at the highest incident energy of 17.5 eV. Indeed, the model was extremely successful to reproduce the near-threshold structure in the angle-integrated metastable excitation function [16].

Finally, Ballance and Griffin [17] recently extended the standard *R*-matrix method with orthogonal orbitals by including a large number of pseudo-states in both the discrete and continuum target spectrum to account for coupling to the high Rydberg states and to the ionization continuum. A total of 397 terms arising from the $3p^6$, $3s^2 3p^5 nl$ and $3s3p^6 nl$ configurations were included in their CI expansion of the target. In order to handle the large number of channels, however, this *R*-matrix with pseudo-states (RMPS) calculation was performed in *LS*-coupling, i.e., relativistic effects were entirely neglected. While such a model would be highly problematic for transitions to the individual members of the $3p^5 4s$ manifold, particularly to the two states with total electronic angular momentum $J = 1$ that need to be described in an intermediate coupling scheme [3], one can still expect the predictions from this approach to be accurate when comparing to the present experimental data as a sum over all four excited states. In fact, the method should be most accurate for the 17.5 eV case, where there are no resonance effects and the slightly different excitation thresholds for the four target states should be least important.

As mentioned before, to enable a direct comparison of the present unresolved experimental results with theory to be made, the theoretical cross sections of all calculations were summed over the four individual transitions to the excited $3p^5 4s$ states.

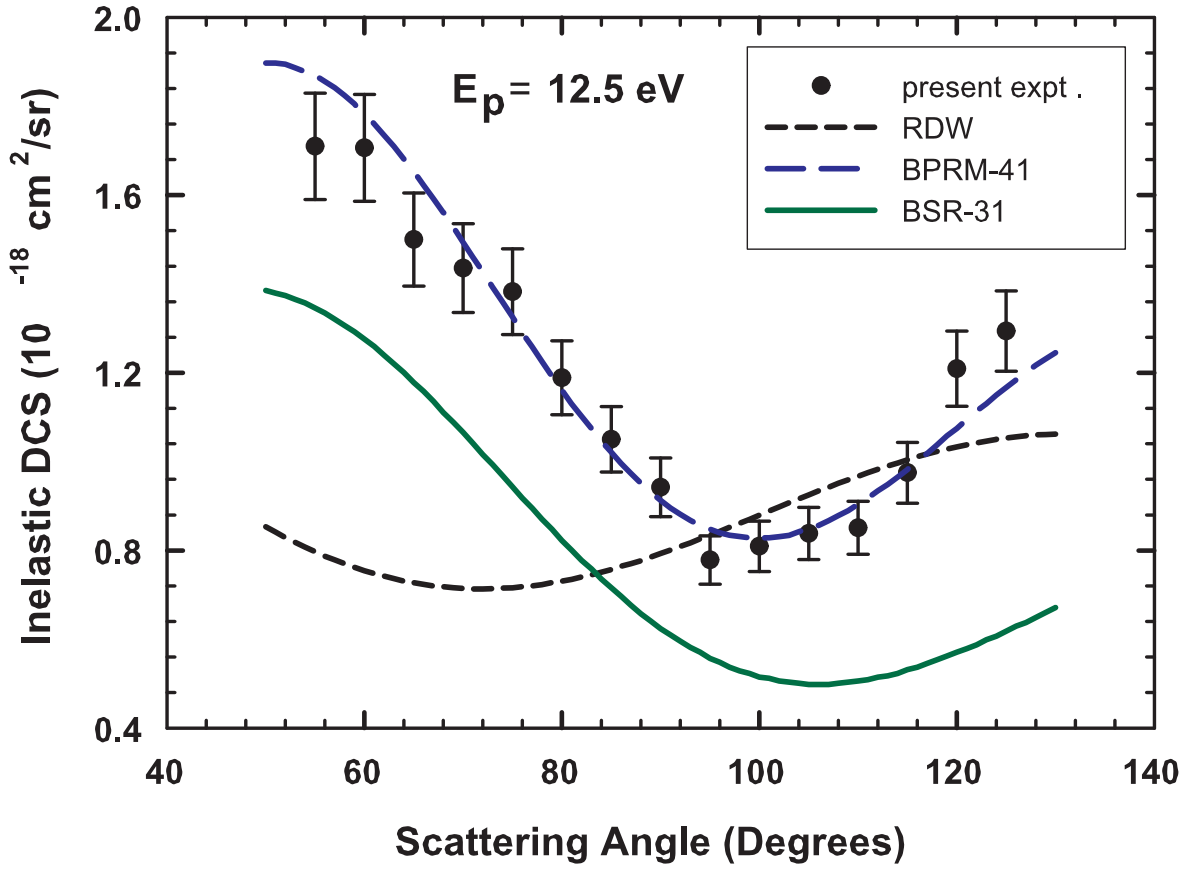

Figure 1
DCS at a projectile electron energy of 12.5 eV. Results for the electron-impact-induced excitation of the summed $3p^5 4s$ states in Ar. Experiment: solid circles, RDW: short-dashed line, BPRM-41: long-dashed line, BSR-31: solid line.

2.3 Comparison of theory with experiment

Figure 1 shows the present experimental DCS data at the nominal impact energy of 12.5 eV compared to the RDW, BPRM-41, and BSR-31 predictions. At this energy, excellent agreement is observed between the BPRM-41 results and the experimental data, with the calculation reproducing accurately both the shape and the magnitude of the measured DCS. Somewhat surprisingly, the BSR-31 calculation describes very well the shape of the experimental DCS, but the predicted cross sections are about 20 percent lower than those observed experimentally. Being based on the close-coupling expansion, the *R*-matrix approach is expected to perform well in this near-threshold region, where the limited number of physical target states included in the models should not be a severe limitation. In contrast, the RDW calculation underestimates the experimental data by a factor of about 2 for scattering angles below 100 degrees and predicts a minimum around 70°, which is reflected neither in the *R*-matrix results nor in the experimental data. This discrepancy with experiment is not surprising for a perturbative theory, given that higher-order effects are known to become increasingly important near threshold.

Figure 2 exhibits DCS results at an impact energy of 14.0 eV. The present experimental data are compared to RDW, BPRM-41, BSR-31, and RMPS [17] predictions as well as the experimental data of Khakoo *et al* [3] in the angular range where they overlap the present results. Both experiments and all theories predict a pronounced minimum between 75° and 85°. Comparing the present experimental results with the previous, there is overall satisfactory agreement, with most data points overlapping within one or two statistical error bars. The exception is at forward angles where the present experimental data are more strongly forward peaked.

At this energy, the RDW calculation is in much better agreement with the experimental results than the other theories, although at forward angles it underestimates both sets of experimental data, while being closer to the previous than the present results. In contrast, the BPRM-41 model predicts a substantially larger cross section at the angular minimum than the other theories and experiments, but it does predict the rapid rise in the cross section at the smaller angles, which characterizes the present experimental results. The BSR-31 and RMPS calculations show overall a

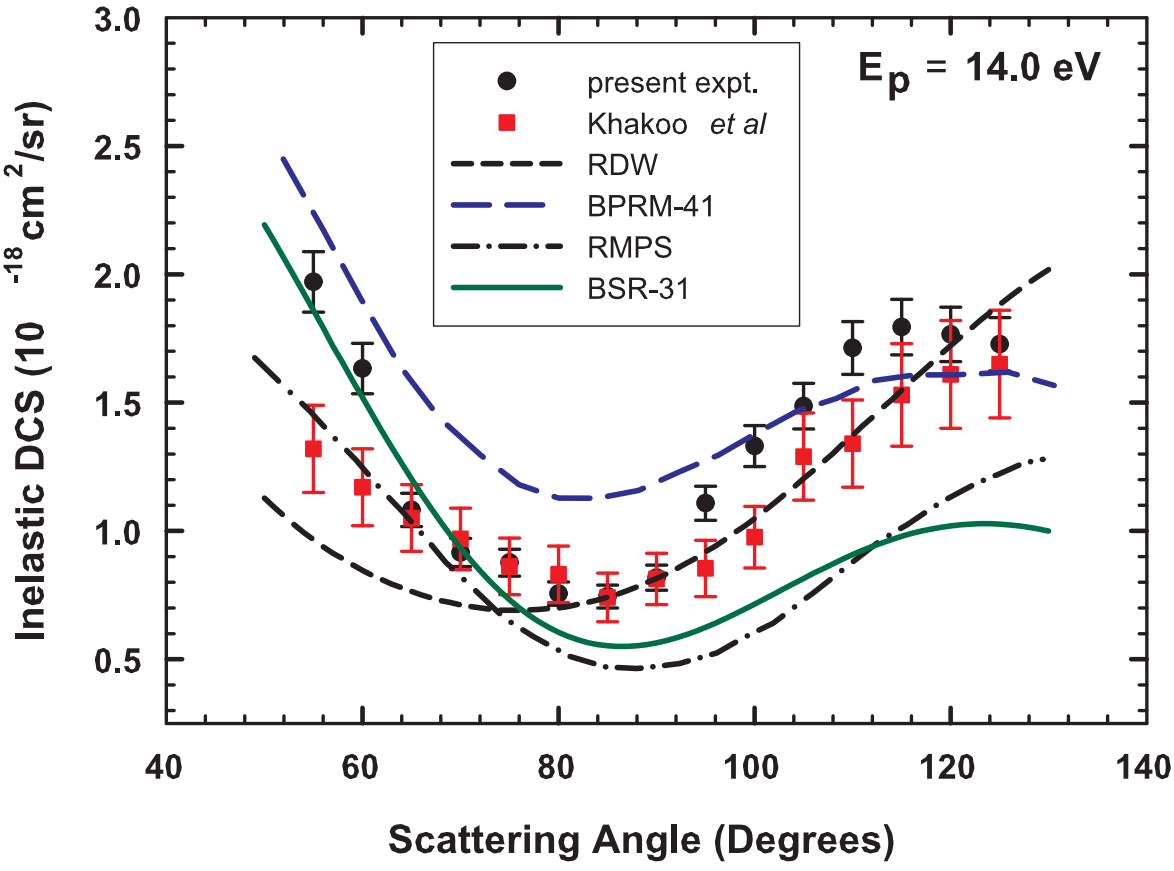

Figure 2
DCS at a projectile electron energy of 14.0 eV. Results for the electron-impact-induced excitation of the summed $3p^5 4s$ states in Ar. Legends as in Figure 1. In addition, the experimental results of Khakoo *et al* [3] (solid squares) and the RMPS calculations of Ballance and Griffin [17] (dash-dot line) are also shown.

greater degree of disparity with the experimental results than the RDW calculation and predict substantially lower cross-section values at the larger scattering angles than the two experiments and the other theories. They are, however, in good agreement with one another, with the BSR-31 calculation more strongly forward-peaked, in agreement with the present experimental data.

Figure 3 displays DCS results for 15 eV incident energy. At this energy there is a significant disparity between the present and previous experimental results. In particular, the local maximum measured around 70° by Khakoo *et al* [3] is neither observed in the present measurement nor predicted by the three calculations. Furthermore, the present measurements yield consistently lower DCS values across the entire angular range than the data of Khakoo *et al* [3]. The RDW results lie between the data of both experiments. Of the three calculations, the BSR-31 and the BPRM-41 predictions are closest to the present experimental results. Similar to the case at 12.5 eV, the BSR-31 model predicts consistently lower DCS values than the other two calculations.

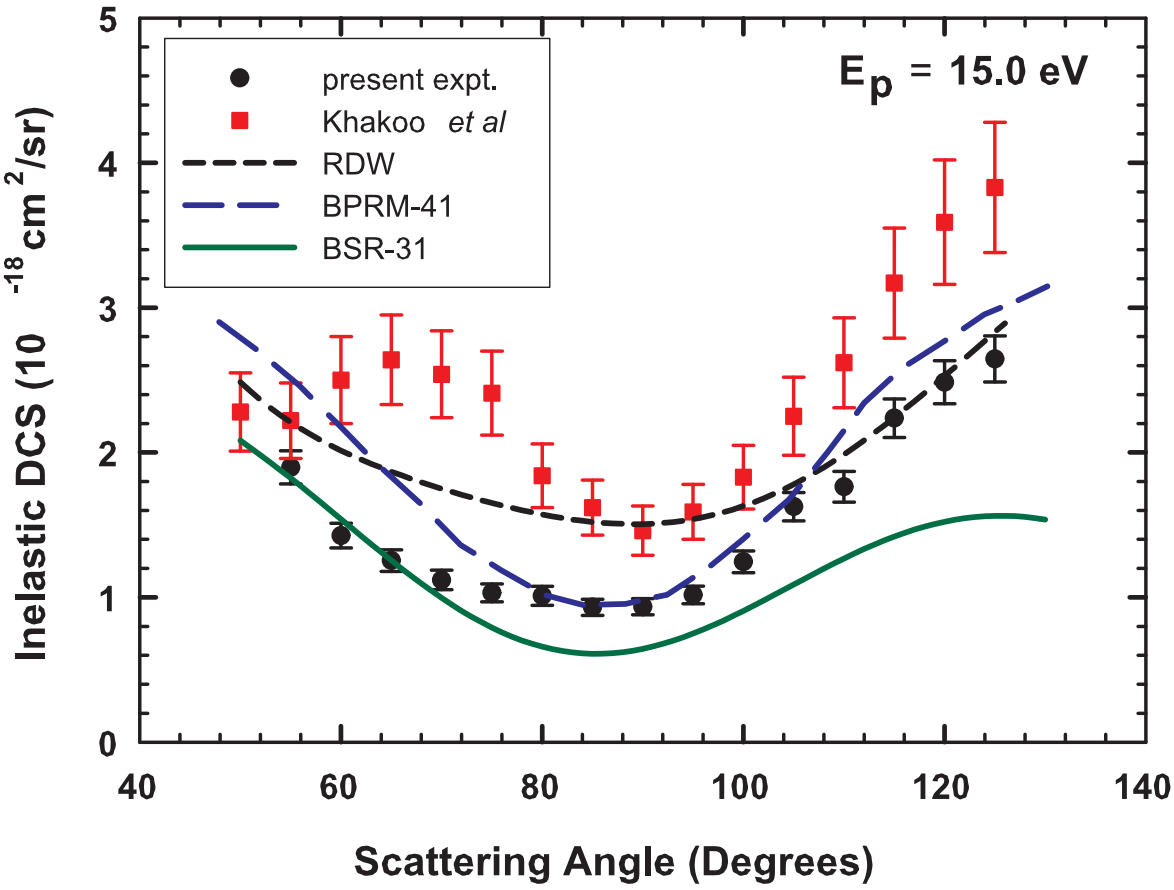

Figure 3
DCS at a projectile electron energy of 15.0 eV. Results for the electron-impact-induced excitation of the summed $3p^5 4s$ states in Ar. Legends as in Figure 2. No RMPS results are available at this impact energy.

Finally, DCS results at 17.5 eV are shown in Figure 4. The present experimental data are again compared to the previous experimental results [3] and the RDW, BPRM-41, BSR-31, and RMPS predictions. In comparing our experimental results with those of Khakoo *et al* [3], the present measurements again are consistently lower and show no sign of a local maximum around 70°, as was the case for 15.0 eV incident energy. Good overall agreement is seen between the present experimental data and the BSR-31 and RMPS results. Particularly at the forward and backward angles, the RMPS calculation provides an excellent description of the present measurements. The BPRM-41 model generally overestimates the present measurements and is in better overall agreement with the previous experimental results, particularly at larger angles. The RDW results are in fair agreement with the data of Khakoo *et al* [3], but are very different from our data and the other three sets of theoretical results, particularly for scattering angles below about 100 degrees.

While the origins of the disparities between the present and the previous experimental results remain unclear, a few possible explanations are proposed. The first is related to different behaviour of the analyzer transmission function $\eta(E_s)$ inherent to the respective spectrometers used in the two measurements. For the present time-of-flight (TOF) spectrometer, due to the absence of electron focussing optics between the interaction region and the detector, an energy-independent electron transmission of value unity is to be expected in the absence of stray fields. Indeed, unity transmission is assumed in the present study. Supporting this assumption are our measurements of the ratio of elastic scattering to excitation of the n = 2 and n = 3 states of helium [12], which were performed with the same apparatus and for which unity transmission was also assumed. In that case the energies of the elastically scattered electrons were up to a factor of 40 times higher than the energies of the inelastically scattered electrons (energies of inelastically scattered electrons down to 0.48 eV, energies of elastically scattered electrons ∼20 eV), i.e., much larger than the corresponding factor of ∼13 for the present measurement. The electron-helium system is easier to treat theoretically than the electron-argon system, and hence theory is expected to be much more reliable in that case. The very good overall agreement achieved between experiment and theory [12] suggests that the assumption of a uniform analyzer transmission was an excellent approximation, one that should be even better for the present measurements due to the smaller dynamic range of scattered electron energies involved. Nevertheless, in spite of our efforts to minimize stray magnetic and electric fields, some small deviation from unity transmission cannot be ruled out, especially at the energies closest to threshold. However, such an error would only affect the absolute scale of the derived DCSs but not their angular dependence.

In contrast, the measurements of Khakoo *et al* [3] employed a dispersive electron analyzer for which large variations in analyzer transmission required correction. The transmission of their analyzer was determined by measuring relative elastic and inelastic DCSs for scattering electrons from helium and by using previous absolute DCS data [18,19]. Their method was similar to that adopted by Nickel *et al* [20]. For projectile electrons of energy 30.58 eV, Nickel *et al* [20] measured the full energy-loss spectrum for helium at a scattering angle of 90°, spanning the range from zero energy loss (elastic scattering) to maximum energy loss (corresponding to a scattered

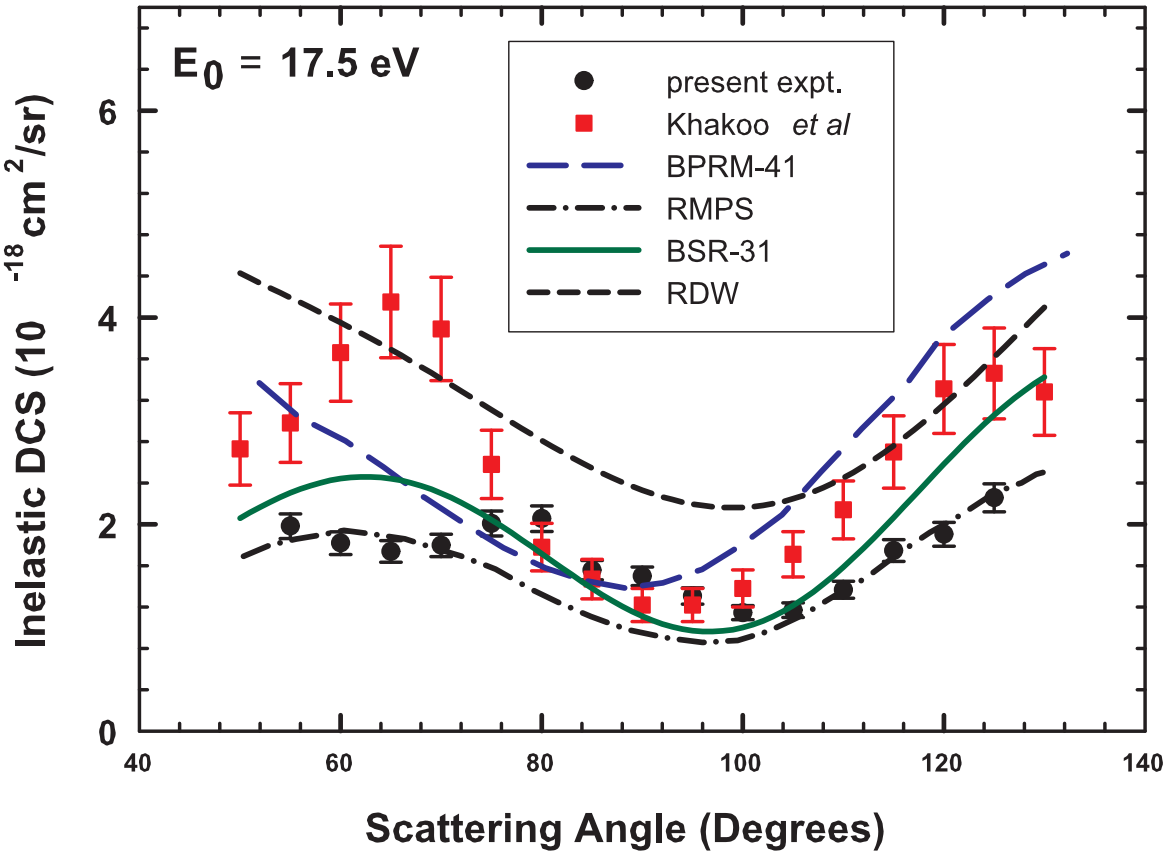

Figure 4
DCS at a projectile electron energy of 17.5 eV. Results for the electron-impact-induced excitation of the summed $3p^5 4s$ states in Ar. Legends as in Figure 2.

electron energy E_s of 0 eV). The measured strengths of the isolated peaks corresponding to elastic scattering (E_s = 30.58 eV), excitation of the n = 2 and n = 3 states ($E_s \sim$ 10 eV and $E_s \sim$ 8 eV, respectively), and the measured strength of the ionization continuum spanning from $E_s \sim$ 6 eV to E_s = 0 eV were compared to previous absolute DCS data [18,19] to determine values for the analyzer-response function $\eta(E_s)$ at specific E_s values. Using interpolation, $\eta(E_s)$ was deduced for all values of E_s between 0 eV and 30.58 eV. We note that the method relies on a number of assumptions and approximations: (i) uniformity of the ionization cross section is assumed in the near-threshold region ($E_s \sim$ 6 eV to E_s = 0 eV) [21] while in reality there is a weak energy dependence; (ii) previous absolute DCS data [18,19] are employed in the determination of $\eta(E_s)$ and thus the deduced energy dependence on E_s is dependent upon the accuracy of those assumed DCS values; (iii) E_s is assumed to be constant between values of 6 eV (the ionization threshold) and ~8 eV (the location of the n = 3 peak), in spite of the fact that $\eta(E_s)$ exhibits a significant degree of energy dependence in other parts of the spectrum. Any breakdown in these assumptions could lead to errors in the determination of the absolute value of the DCSs and to distortions in the

angular behaviour. We note that in contrast to the work Nickel *et al* [20], the helium energy-loss spectrum of [3] was determined at the slightly different incident electron value of 31.7 eV, which will modify the above interpolation procedure to a small degree.

A second possible cause for the disparity could be related to a potentially high sensitivity of the derived cross sections to the value of the incident beam energy in the proximity of resonance structures in the incident-electron scattering channel. Such an effect was observed in our previous measurements on helium [12]. In the vicinity of such resonances, small errors in the experimental energy calibration can potentially lead to large differences in the measured count rates. This should be especially borne in mind when comparing the present and previous argon data at the nominal incident energies of 14.0 eV and 15.0 eV, i.e., energy values in the neighbourhood of the strong resonance structures at 14.054 eV and between 14.98 eV and 15.12 eV [5], respectively. In contrast, the measurement at 12.5 eV is performed in a region of the energy spectrum that is devoid of resonance structures. Also, for the 17.5 eV measurement, no enhanced sensitivity to energy calibration is anticipated due to the lack of strong resonance structures in that energy regime.

Other possible sources of experimental error can arise from the subtraction of stray-electron contributions from the data, which may introduce systematic errors. For example, for both experiments the adopted subtraction procedures will not account for contributions from any electrons first scattering from the primary beam and subsequently scattering from surrounding surfaces before entering the electron spectrometer, or for space-charge-related changes in beam focussing due to removal of the target beam from the interaction region during background runs. While such contributions are likely to be small, they nevertheless represent possible sources of error.

3. Conclusions

We have presented absolute differential cross section (DCS) data for the excitation of the $3p^5 4s$ manifold in argon by electron impact. The study focuses on the near-threshold region where previous studies have revealed persistent disparities between measurements and theoretical predictions. Through the application of improved experimental techniques, the aim of this work was to seek closing the gap between experiment and theory.

The experimental results were derived using the time-of-flight technique. In contrast to the methods employed previously, this technique allows for the relative strength of elastic and inelastic features in an energy-loss spectrum to be directly related, without the need to correct for energy-dependent variations in analyzer transmission. In this way, a potential source of error in the determination of DCS data is removed. In addition, the present measurements extend much closer (~1 eV) to the excitation threshold than work reported previously.

Calculations were performed using an improved version of the relativistic distorted-wave method, as well as two versions of the semi-relativistic *R*-matrix approach. These results were compared to the present data and to selected recent experimental and theoretical results by other groups in the angular range where they overlap with the present kinematics.

At the lowest impact energy of 12.5 eV (~1 eV) from threshold, there is excellent agreement between a standard 41-state Breit-Pauli *R*-matrix calculation and the present experimental results. However, this high level of agreement is probably accidental, since it is not reproduced by this model at the larger impact energies. At 12.5 eV the RDW model severely underestimates the cross section at smaller angles, but performs better as the incident energy is increased. The recent non-relativistic RMPS results of Ballance and Griffin [17] are very close to the present measurements at 17.5 eV, but not at 14.0 eV. As one might have expected, the predictions of the BSR-31 and RMPS calculations are close to one another, with both generally predicting lower DCS values than the other two theories.

Overall, no clear trends are observed in the degree of agreement between the various theories and experiments as a function of impact energy. Significant disparities remain between all theories and the experimental data presented here. This finding once again highlights the challenges posed in the near-threshold region and underlines the need for further improvements in both theoretical and experimental techniques. Given the good agreement between the BSR-31 and RMPS predictions, both of which would generally be expected to be appropriate models for the problem at hand, it is not immediately obvious where the theoretical problems might lie. In light of the advances in computer hardware and software, we expect to be in a position to perform Breit-Pauli or even Dirac-Coulomb RMPS calculations within the next few years to further investigate this problem.

Acknowledgements

The authors acknowledge funding from the Australian Research Council under the Centres of Excellence Programme. The work of KB and OZ is supported by the United States National Science Foundation under grants PHY-0757755 and PHY-0903818.

References

1. Filopovic DM, Marinkovic BP, Pejcev V, Vuskovic L: *Journal of Physics B: Atomic, Molecular and Optical Physics* 2000, **33:**677-691.
2. Filipovic DM, Marinkovic BP, Pejcev V, Vuskovic L: *Journal of Physics B: Atomic, Molecular and Optical Physics* 2000, **33(11):**2081-2094.
3. Khakoo MA, Vandeventer P, Childers JG, Kanik I, Fontes CJ, Bartschat K, Zeman V, Madison DH, Saxena S, Srivastava R, Stauffer AD: *Journal of Physics B: Atomic, Molecular and Optical Physics* 2004, **37:**247-281.
4. Lange M, Matsumoto J, Setiawan A, Panajotović R, Harrison J, Lower JCA, Newman DS, Mondal S, Buckman SJ: *Review of Scientific Instruments* 2008, **79(4):**043105.
5. Buckman SJ, Hammond P, King GC, Read FH: *Journal of Physics B: Atomic and Molecular Physics* 1983, **16(22):**4219-4236.
6. LeClair LR, Trajmar S, Khakoo MA, Nickel JC: *Review of Scientific Instruments* 1996, **67(5):**1753-1760.
7. Srivastava SK, Tanaka H, Chutjian A, Trajmar S: *Phys Rev A* 1981, **23(5):**2156-2166.

8. Panajotovic R, Filipovic D, Marinkovic B, Pejcev V, Kurepa M, Vuskovic L: *Journal of Physics B: Atomic, Molecular and Optical Physics* 1997, **30(24):**5877-5894.
9. Furst JE, Golden DE, Mahgerefteh M, Zhou J, Mueller D: *Phys Rev A* 1989, **40(10):**5592-5600.
10. DuBois RD, Rudd ME: *Journal of Physics B: Atomic and Molecular Physics* 1976, **9(15):**2657-2667.
11. Williams JF: *Journal of Physics B: Atomic and Molecular Physics* 1979, **12(2):**265-282.
12. Lange M, Matsumoto J, Lower J, Buckman S, Zatsarinny O, Bartschat K, Bray I, Fursa D: *Journal of Physics B: Atomic, Molecular and Optical Physics* 2006, **39(20):**4179-4190.
13. Khakoo MA, Wrkich J, Larsen M, Kleiban G, Kanik I, Trajmar S, Brunger MJ, Teubner PJO, Crowe A, Fontes CJ, Clark REH, Zeman V, Bartschat K, Madison DH, Srivastava R, Stauffer AD: *Phys Rev A* 2002, **65(6):**062711.
14. Zuo T, McEachran RP, Stauffer AD: *Journal of Physics B: Atomic, Molecular and Optical Physics* 1991, **24(12):**2853-2870.
15. Bartschat K, Zeman V: *Phys Rev A* 1999, **59(4):**R2552-R2554.
16. Zatsarinny O, Bartschat K: *Journal of Physics B: Atomic, Molecular and Optical Physics* 2004, **37(23):**4693-4706.
17. Ballance CP, Griffin DC: *Journal of Physics B: Atomic, Molecular and Optical Physics* 2008, **41(6):**065201.
18. Trajmar S, Register DF, Cartwright DC, Csanak G: *Journal of Physics B: Atomic, Molecular and Optical Physics* 1992, **25(22):**4889-4910.
19. Register DF, Trajmar S, Srivastava SK: *Phys Rev A* 1980, **21(4):**1134-1151.
20. Nickel JC, Zetner PW, Shen G, Trajmar S: *Journal of Physics E: Scientific Instruments* 1989, **22(9):**730-738.
21. Wannier GH: *Phys Rev* 1953, **90(5):**817-825.